# Study of the amorphous and crystalline states in Ge(Te1-xSex) thick films (x = 0, 0.50) by in situ temperature-dependent structural analyses

P. Armand, G. Silly, R. Escalier, J. Lizion, C. Mocuta, A. Piarristeguy

▶ **To cite this version:**

P. Armand, G. Silly, R. Escalier, J. Lizion, C. Mocuta, et al.. Study of the amorphous and crystalline states in Ge(Te1-xSex) thick films (x = 0, 0.50) by in situ temperature-dependent structural analyses. Journal of Alloys and Compounds Communications, 2024, 2, pp.100004. 10.1016/j.jacomc.2024.100004 . hal-04575593

**HAL Id: hal-04575593**
**https://hal.science/hal-04575593**

Submitted on 15 May 2024

**HAL** is a multi-disciplinary open access archive for the deposit and dissemination of scientific research documents, whether they are published or not. The documents may come from teaching and research institutions in France or abroad, or from public or private research centers.

L'archive ouverte pluridisciplinaire **HAL**, est destinée au dépôt et à la diffusion de documents scientifiques de niveau recherche, publiés ou non, émanant des établissements d'enseignement et de recherche français ou étrangers, des laboratoires publics ou privés.

# Study of the amorphous and crystalline states in $Ge(Te_{1-x}Se_x)$ thick films ($x$ = 0, 0.50) by *in situ* temperature-dependent structural analyses.

P. Armand[1,*], G. Silly[1], R. Escalier[1], J. Lizion[1], C. Mocuta[2], A. Piarristeguy[1]

[1]: ICGM, Univ Montpellier, CNRS, ENSCM, Montpellier, France

[2]: Synchrotron SOLEIL, L'Orme des Merisiers, Départementale 128, 91190 Saint-Aubin

*Corresponding author: pascale.armand@umontpellier.fr

| | | |
|---|---|---|
| ORCID: | P. Armand | 0000-0001-8921-5427 |
| | A. Piarristeguy | 0000-0002-8922-4566 |
| | C. Mocuta | 0000-0001-5540-449X |
| | G. Silly | 0000-0001-8212-2359 |
| | J. Lizion | 0000-0001-9433-5394 |
| | R. Escalier | 0000-0003-4179-804X |

**Abstract:**

As-deposited and unencapsulated $GeTe_{1-x}Se_x$ ($x$ = 0, 0.5) 3-µm-thick amorphous films on Si(001) were obtained via the thermal co-evaporation technique. The crystallization and the structure of these phase change materials were examined using *in situ* temperature-dependent X-ray diffraction (XRD) and grazing-incidence fluorescence X-ray Absorption Near Edge Structure (XANES) in isochronal annealing conditions under nitrogen flow. The results show that the onset temperature of crystallization is highly sensitive to the substitution of the Te atoms by the Se ones and that the rhombohedral structure, with the space group *R*3*m*, is the one that crystallized for both samples without Ge or Te rejection. Moreover, the local order around the Ge and Se atoms, probed by Ge and Se K-edge XANES analyses, presents clear modifications from the amorphous state to the crystalline one expecting a Ge four-fold and a Se two-fold coordination in the amorphous state, with an increase of the local disorder with the Se substitution ($x$ = 0.5).

**Keywords**: X-ray diffraction; GeTe; X-ray Absorption Near Edge Structure (XANES); Phase Change Material (PCM); X-ray absorption; Crystallization kinetic.

## 1. Introduction

Phase change materials (PCMs) have emerged as a remarkable class of materials due to their potential applications in various fields, including data storage, thermal management, and electronics. One such fascinating PCM is germanium telluride GeTe, which has garnered considerable interest due to its exceptional phase change properties and its potential for use in advanced technologies. GeTe undergoes a fast and reversible structural phase transition between the crystalline and amorphous states upon applying heat via electrical or optical pulses. The transition between these phases results in a significant change in the physical properties, such as electrical conductivity, optical reflectivity, and thermal conductivity [1–3].

α-GeTe crystallizes in a rhombohedral system, stable at ambient conditions, with an acentric $R3m$ space group (N° 160, $C_{3v}^5$, $Z = 3$) forming distorted octahedra $GeTe_6$ having 3 short (2.83 Å) and 3 long (3.16 Å) Ge-Te bonds [4]. To explain its uncommon physical properties compared to the other types of GeTe symmetry, the existence of polarizable Ge−Te "metavalent-like bonds" (MVB), an electron-deficient bond, has been reported in α-GeTe [5–7]. The crystallization temperature $T_c$ for α-GeTe films is also an important parameter to consider, as introducing the amorphous film into the PCM system requires a brazing process that brings heat to the system and consequently to the film. Reported $T_c$ values of as-deposited GeTe films are dependent on the exact composition of the film, the film thickness, the deposition technique, the air protection (capping), the heating rate, etc... [8–11].

To develop useful alloys for PCM applications, experimental works have demonstrated that the partial substitution of Te atoms by Se ones in rhombohedral compositions synthesized in the GeTe–GeSe pseudo-binary has emphasized the phase change properties [11–15]. For example, a $GeTe_{0.9}Se_{0.1}$ as-deposited 500 nm-thick film presents a resistance contrast between its

amorphous and crystalline states of more than seven orders of magnitude compared to the one reported for GeTe [15]. Ren *et al.* [11] observed a fast (500 ns) and reversible electrical switching at about 270 °C for the 200 nm-thick $GeTe_{0.74}Se_{0.26}$ film with good data retention of 10 years at 208.5 °C. According to the phase equilibria in the GeTe-GeSe pseudo-binary system established from bulk samples, the $GeTe_{1-x}Se_x$ alloys with $x \leq 0.5$ crystallized in a rhombohedral system stable at ambient conditions with an acentric *R*3*m* space group [16–18]. This paper explores the effect of the partial substitution of Te atoms by Se atoms in the rhombohedral structure on the crystallinity and the crystallization temperatures due to thermal energy input for $GeTe_{1-x}Se_x$ 3-µm thick films with $x = 0$, 0.5. The temperature-dependent grazing incidence X-ray scattering patterns and the X-ray Absorption Near Edge Structure (XANES) spectra were collected simultaneously in isochronal annealing conditions at the DiffAbs beamline, SOLEIL synchrotron (www.synchrotron-soleil.fr). The local electronic structure and configuration around the absorbing atom strongly influence the XANES spectrum. Thus, the XANES spectroscopy is an appropriate technique to approach the short- and medium-range structure around the probed atom, especially in the amorphous state. The examination of the short-range order in the amorphous state of the PCM chalcogenide-based material was the subject of several publications, as it would play an important role in the variation of the phase change properties between the crystallized and the amorphous states [19–21]. The fluorescence collected-XANES spectra at Ge and Se K-edges upon continuing heating conditions allow us to study their crystallization, particularly their crystallization kinetic, which is another important parameter that influences the resistivity behavior.

## 2. Experimental section

### *2.1 Samples synthesis*

The $GeTe_{1-x}Se_x$ ($x$ = 0, 0.5) 3-μm thick amorphous films deposited on a Si(001) substrate were obtained via the thermal co-evaporation technique of the pure elements (Ge pieces from Goodfellow, Te pieces, and Se granules from ChemPur, each one with a purity of 99.999%) using a PLASSYS MEB 500 device. During deposition, the substrate holder was rotated at 8 rpm to get uniform film thickness and heated at 90 °C to improve the adhesion with the deposited layer. Details on the experimental conditions were already given [22]. Their as-deposited amorphous state was checked via room-temperature X-ray scattering experiments using a Panalytical X'Pert diffractometer using the Cu Kα excitation line. The thick films were characterized without capping layers as it has been shown, for GeTe films thicker than 50 nm, that the characteristic temperatures are not affected by oxidation [23].

The α-GeTe and α-$GeTe_{0.5}Se_{0.5}$ bulk samples used as references were synthesized by classical synthesis routes from high-purity chemical elements. For the ternary composition, the precursors GeTe and GeSe were first synthesized. The sealed silica tube containing about 1g of (Ge + Te) or (Ge + Se) powders was heated at a low heating rate of 10 °C/h until around 950 °C, using a rocking furnace to form a homogeneous melt. After 4 hours at 950 °C, the rocking was stopped, and the tubes were cooled down to room temperature at a rate of 10 °C/h. The GeTe and GeSe ingots were crushed and ground into a fine powder in an agate mortar, then sieved with a 125 μm sieve. The powdered GeTe and GeSe were mixed in the proportions required to obtain the $GeTe_{0.5}Se_{0.5}$ composition and the same heating treatment used to form the precursors was applied.

*2.2 Characterizations*

The chemical composition of each deposited film was measured at room temperature, before and after heat treatment, by energy-dispersive X-ray (EDX) spectroscopy with a Zeiss EVO HD15 instrument equipped with an Oxford Instruments X-Max N Si drift detector (SDD) EDX. EDX analysis is a semi-quantitative method that allows probing to a depth of about 1 μm.

Temperature-dependent grazing incidence fluorescence and X-ray scattering patterns were collected simultaneously *in situ* on the DiffAbs beamline at SOLEIL Synchrotron (Saint-Aubin, France). The details of the experimental setup and furnace characteristics can be found in a previous paper [22]. The sample was placed on a heating stage, held by a system of clips, and heated by thermal contact. A thermocouple encapsulated in the heating plate measures the temperature in real time. The furnace was mounted on a six-circle diffractometer, and the grazing incident angle ω was fixed to 6°. The X-ray photon energy was set to 11.015 keV (λ = 1.1256 Å) using a double-crystal Si(111) monochromator (with an energy resolution $\Delta E/E = 10^{-4}$). The X-ray beam was focused vertically and horizontally to a size of about 200 × 250 μm (full width at half maximum, FWHM), using a longitudinal bend mirror and the sagitally bent second crystal of the monochromator, respectively. Two mirrors ensure harmonics rejection of about $10^{-6}$. During heating, the samples were kept under a nitrogen-protective atmosphere.

The elastic X-ray scattered signal was detected using an XPAD-S140 two-dimensional hybrid pixel detector [24, 25] placed behind the sample at a distance of typically 200–300 mm to intercept diffraction rings over an angular range of approximately 7° in scattering angle ($2\theta$). Several images were collected along the $2\theta$ angle by moving the detector to extend the available $2\theta$ domain. The incident beam intensity $I_0$ was also monitored and recorded during the whole experiment. The fluorescence signal was recorded using a 4-element Silicon drift detector (SDD) Vortex®-4ME from Hitachi, with an active area of 4 ×50 $mm^2$ and a typical energy

resolution of ~150 eV, resulting in collections of full energy spectra. Regions of Interest (ROIs) around the characteristic K-lines of Ge and Se were used to obtain the XANES signal. To reduce the acquisition times, the fluorescence-type XANES spectra were recorded at the Ge K-edge and Se K-edge using a variable energy step, Table I.

**Table I:** Energy ranges and steps used for the acquisitions of the XANES spectra.

| **Energy steps (eV)** | **Energy range (eV)** | |
|---|---|---|
| | **Ge K-edge (11104 eV)** | **Se K-edge (12658 eV)** |
| **5** | 11015 – 11070 | 12575 – 12625 |
| **0.5** | 11070 – 11136 | 12625 – 12687 |
| **1** | 11136 – 11226 | 12687 – 12778 |

For the GeTe thick film, the *in-situ* temperature-dependent data measurement loop from 25 to 155 °C consisted of 3 × [XRD pattern of 30 sec. each with a 2θ step of 0.0115°] followed by one Ge K-edge XANES spectrum (2 sec/point, 8 min./full spectrum). The experimental data were recorded continuously during the temperature ramps. The temperature ramp was 20 °C/min from 25 to 90 °C then, 0.2 °C/min up to 155 °C. Before each sequence, the sample surface was automatically realigned. The same procedure was followed for the ternary film $GeTe_{0.5}Se_{0.5}$, but the XANES data recording at the Se K-edge (2 sec/point, 8 min./full spectrum) was added to the loop, and the maximum reached temperature was 300 °C. The temperature ramp was 20 °C/min from 25 to 215 °C then, 0.2 °C/min up to 300 °C.

Each powdered reference (α-GeTe and α-$GeTe_{0.5}Se_{0.5}$) was introduced into a 0.5 mm diameter borosilicate capillary, which was then air-sealed. Only room-temperature XANES data at the Ge K-edge and Se K-edge were recorded.

The XANES spectra were normalized in absorbance by i) fitting the raw data in the pre-edge region (90 to 30 eV before the edge step $E_0$) with a first-order polynomial extrapolated through the post-edge region and subtracting this as background absorption, ii) normalizing for atomic

absorption, based on a second-order polynomial of the spectral region after the edge, from 15 to 120 eV from $E_0$, iii) subtracting the pre-edge line from the entire spectra and dividing the entire spectra by the absorption edge step. The edge step was evaluated by taking the difference between the pre-edge and normalization lines at $E_0$. The value of $E_0$ was taken at the maximum of the first derivative curve.

## 3. Results

### *3.1 GeTe film*

#### *3.1.1 Temperature-dependent X-ray scattering patterns*

The amorphous as-deposited undoped GeTe thick film presents a Ge / Te ratio of 48 / 52 in at. % with an error estimated of ± 3 at. % which, compared to the stochiometric GeTe, corresponds to a slight Te enrichment. The heating temperature-dependent grazing incidence X-ray scattering patterns were recorded using a monochromatic beam (wavelength λ of 1.1256 Å) and are shown in Figure 1. From room temperature to 124 °C, the film is amorphous (zone I). With our experimental conditions, the 3μm-thick GeTe film's temperature crystallization onset is 124 °C ($T_c$). Zone II contains the amorphous and crystalline states of the GeTe film, while only the crystalline state is present in zone III, Figure 1(a). Figure 1(b) presents *in situ*-collected X-ray scattering patterns at selected temperatures. At T = 130 °C, the pattern is the combination of scattering rings due to the main amorphous part of the film with small intensity diffracted peaks. All the XRD lines are present at T= 136 °C and the diffraction profiles remain stable up to the final recorded temperature, T = 154 °C.

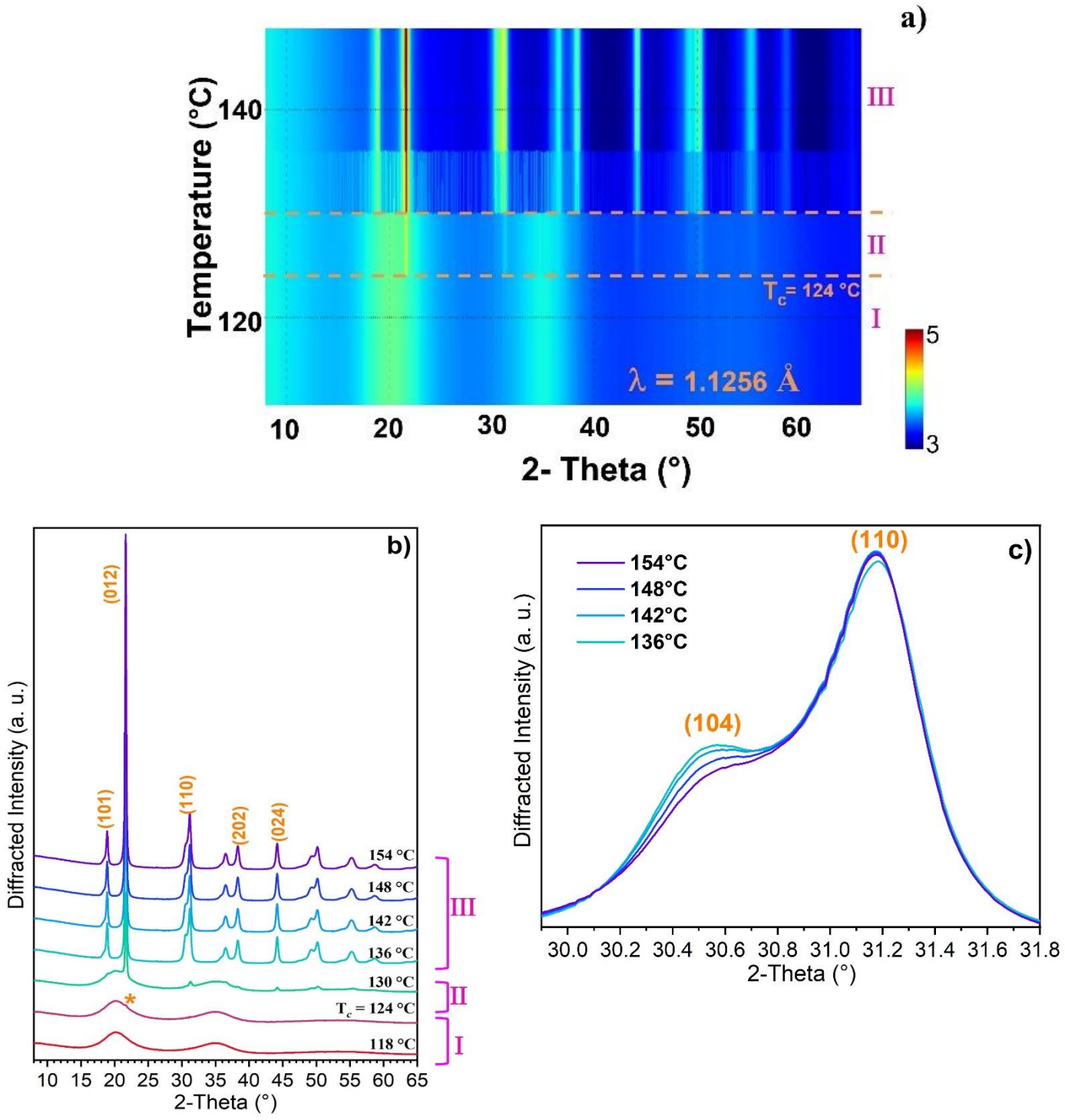


**Figure 1:** a) *In-situ* temperature-dependent synchrotron X-ray scattering patterns recorded for a GeTe 3-µm-thick film on a Si(001) substrate in isochronal annealing conditions (log color scale), b) X-ray scattering patterns at selected temperatures (Y scale is linear, stacked and vertically shifted for clarity). The star pointed out the emergence of a diffraction peak at the onset of crystallization ($T_c$ temperature). c) enlarged $2\theta$ range for the (110) peak, highlighting the evolution of a (104) shoulder.

The as-deposited 3-μm-thick GeTe film crystallizes within the well-known rhombohedral-type symmetry, one of the GeTe polymorphs with acentric *R*3*m* space group (*Z* = 3, N° 160), according to the Ge-Te equilibrium phase diagram [16–18]. The 2D van der Waals layered α-GeTe crystalline structure can be described as a distorted cubic structure with Te atoms having a formal charge of 2-, and $Ge^{II}$ atoms located in 3*a* Wyckoff sites [7]. Both Ge and Te atoms are six-fold coordinated in their first shell forming quasi-octahedra $GeTe_6$ ([3+3] shell) with three short and three long Ge-Te bonds [4, 13].

The diffraction peaks are indexed using the simplest multiple (M = 3) hexagonal unit cell. Instead of using the (*hkil*) notation, we used only the three indices notation (*hkl*) as regularly found in the literature on GeTe-based PCMs. The (012) Bragg line is the most intense and no impurities crystallized phase or segregation into elemental Ge/Te were identified in Figure 1.

In the temperature range of 136 – 154 °C, the angle positions for all the diffraction peaks appear rather constant (within the small drifts due to the thermal expansion of the unit cell), Figure 1. We notice that the diffraction peaks are wide, Figure 1(b), which could be attributed to a crystalline grain size effect and/or micro-strains. With the hypothesis that only the size of the crystallites is responsible for the widening of the diffraction peaks, Debye-Scherrer's law can be used. It relates the average diameter *D* of spherical crystallites to the Full Width at Half Maximum (FWHM) of a diffracted peak according to the following equation:

$$D = [0.89 \times \lambda] / [B \times \cos(\theta)],$$

where *B* is the FWHM of the peak in radian, $\lambda$ is the wavelength in nm (0.11256 nm for this work), and $\theta$ the half-angle maximum position of the peak.

The half-angle position $\theta$ of the (012) dominant peak in Figure 1 slightly decreases with the increase of the temperature leading to an increase of the inter-reticular distance $d_{012}$, Table II. The average grain size *D* of the diffracting domains (~ 24 nm) stays rather constant (within the error bar) with the heating temperature in the explored temperature range ($\Delta T \approx 20$ °C).

**Table II:** Temperature-dependent half-angle position of the (012) main XRD peak obtained on the α-GeTe thick film with a wavelength λ of 1.1256 Å, its FWHM, and the calculated *D* parameters. The instrument resolution function (~ 0.02 - 0.03° in 2-theta) was not deconvoluted from the measurements. The incertitudes are given in parentheses.

| **T (°C)** | **θ (°) (012) peak** | **FWHM (rad) (012) peak** | ***D* (nm)** |
|---|---|---|---|
| **136** | 10.83(1) | 0.0042(4) | 23.43(1) |
| **142** | 10.82(1) | 0.0040(4) | 24.60(1) |
| **148** | 10.82(1) | 0.0041(4) | 24.00(1) |
| **154** | 10.82(1) | 0.0042(4) | 23.43(1) |

Figure 1(c) highlights the rather constant angle position of the (110) Bragg line and its slight intensity augmentation from 136 to 154 °C. In the same temperature range, the intensity of the (104) diffracted peak diminishes and its maximum angle position tends to shift to the higher 2θ implying a decrease in the $d_{104}$ inter-reticular plan's distance, Table III.

**Table III:** Temperature-dependent half-angle (θ) positions (on continuing heating) of two selected diffracted peaks obtained with a wavelength λ of 1.1256 Å on the α-GeTe film, with the corresponding inter-planar distances $d_{hkl}$, the *c*, and *a* cell parameters, the *c*/*a* ratio, and the cell volume *V*. The incertitudes are given in parentheses.

| **T°** | **136 °C** | | | **142 °C** | | | **148 °C** | | | **154 °C** | | |
|---|---|---|---|---|---|---|---|---|---|---|---|---|
| **(*hkl*)** | **θ (°)** | **$d_{hkl}$ (Å)** | ***c*, *a* (Å)** | **θ (°)** | **$d_{hkl}$ (Å)** | ***c*, *a* (Å)** | **θ (°)** | **$d_{hkl}$ (Å)** | ***c*, *a* (Å)** | **θ (°)** | **$d_{hkl}$ (Å)** | ***c*, *a* (Å)** |
| **(*104*)** | 15.25(1) | 2.14(4) | 10.60(8) (*c*) | 15.25(1) | 2.14(4) | 10.60(8) (*c*) | 15.25(1) | 2.14(4) | 10.60(8) (*c*) | 15.26(1) | 2.14(4) | 10.58(8) (*c*) |
| **(*110*)** | 15.59(1) | 2.09(4) | 4.18(8) (*a*) | 15.59(1) | 2.09(4) | 4.19(8) (*a*) | 15.59(1) | 2.09(4) | 4.19(8) (*a*) | 15.59(1) | 2.09(4) | 4.18(8) (*a*) |
| ***c* / *a*** | 2.53 | | | 2.53 | | | 2.53 | | | 2.53 | | |
| ***V*** **(Å³)** | 161.0(2) | | | 161.0(2) | | | 161.0(2) | | | 160.8(2) | | |

The *a* and *c* cell parameter values and the volume *V* of the rhombohedral structure of α-GeTe, given in Table III, were obtained from $d_{110}$ and $d_{104}$ Bragg lines according to equations [8]:

$$a\ (\text{Å}) = 2\times d_{110} \qquad \text{Eq. 1}$$

$$c\ (\text{Å}) = \frac{4d_{110}}{\sqrt{-\frac{1}{3}+\left(\frac{d_{110}}{d_{104}}\right)^2}} \qquad \text{Eq. 2}$$

$$V\ (\text{Å}^3) = a^2\times c\times \sin(120°) \qquad \text{Eq. 3}$$

With heating, the *c* parameter, both the *c* /*a* ratio and the volume diminish slightly while the *a* parameter values stay rather constant in this 136 – 154 °C temperature domain, Table III.

### *3.1.2 Temperature-dependent XANES spectra*

Simultaneously with the temperature-dependent XRD data collection, the *in-situ* fluorescence-detected XANES signals of the as-deposited GeTe film were registered around the Ge K-edge with the isochronal annealing conditions. XANES is a local sensitive, chemical selective probe that may provide structural, and electronic details. The energy position of the edge of a given chemical element is characteristic of its considered electronic level (K, L..), and its oxidation state. The ground state electronic configuration of the atomic Ge is $[Ar]4s^2 3d^{10} 4p^2$ and its outer

shell electronic configuration is $4s^2 4p_x^1 p_y^1 p_z^0$ [11]. In a compound, germanium can engage its four valence electrons in bonds with its first neighbors. It is then in a formal oxidation state (+IV). In the oxidation state (+II) only the two electrons of the 4*p* orbitals participate in the formation of bonds and the two paired and unengaged 4*s* electrons form a pair called a "lone pair" or "E pair".

In a solid, the resonant XANES features close to the energy of the core excitation level are related to the electronic structure with dipole transitions from the excited core level to local unoccupied bands in the density of states (empty-DOS). In the case of semiconductors, it provides information on the conduction band (CB) states. Ge K-edge XANES of GeTe reflects the 4*p* electronic structure through the partial density of unoccupied states.

Three distinctive experimental spectral shapes are visible in Figure 2(a). The one, from 107 to 124 °C, corresponds to the amorphous state of GeTe (zone I in Figure 1). The second, from 136 °C to the highest registered temperature of 154 °C (zone III in Figure 1), is due to the rhombohedral structure. The third distinctive spectral shape at T = 130 °C (Zone II) is the combination of the XANES shape of the amorphous and the crystalline states. Figure 2(b) presents a selection of XANES spectra representative of the three distinctive shapes compared with the XANES curve of the powdered crystalline α-GeTe, used as a reference, contained in a capillary tube and registered at 25 °C. The Ge K-edge XANES spectrum of the undoped GeTe thick film registered at the highest temperature (T = 154 °C), *i.e.*, in the temperature domain of the crystallized state (zone III), closely resembles the reference α-GeTe obtained in the bulk form, see Figure 2(b). In α-GeTe, Ge carries a formal charge of 2+. As the total of the *p*-electrons for Ge and Te is 6, their *p* bands are half unoccupied [11]. The broader features observed for the XANES spectra in the amorphous state are due to the inherent disordered nature of glasses, which have a broad range of Te-Ge-Te angles and Ge-Te distances compared to crystalline materials.

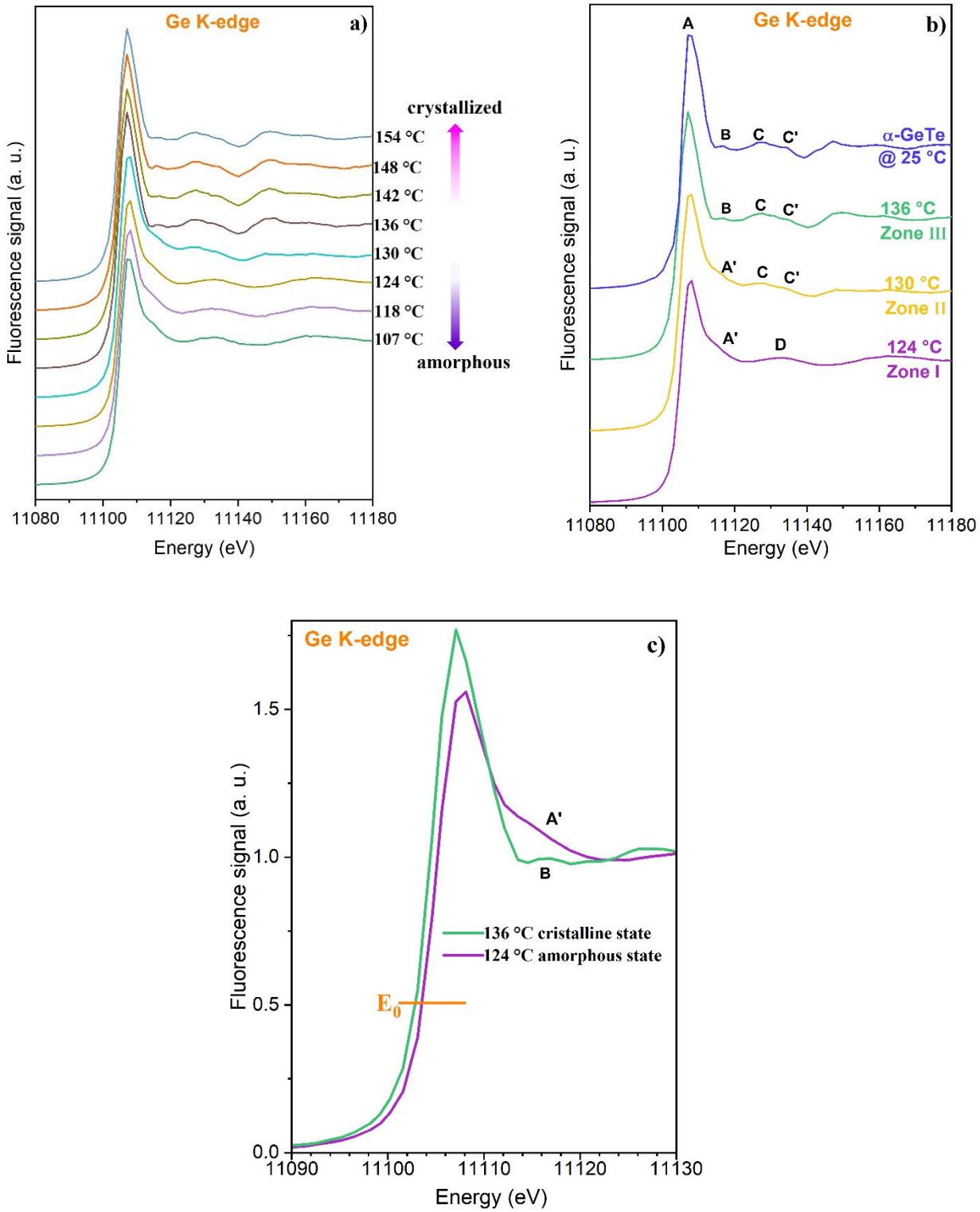


**Figure 2:** a) Evolution with the temperature of the near-edge features in the normalized fluorescence (at the unit edge jump) spectra of the as-deposited GeTe film, b) fluorescence spectra at selected temperature compared to that of the powdered reference (bulk) α-GeTe (*R*3*m*) registered at ambient conditions (blue curve). The spectra have been stacked and vertically shifted for clarity. c) zoom of the two states (amorphous and crystalline) of the GeTe parent.

The sharp edge, around 11104 eV, arises mainly from the allowed Ge $1s \rightarrow 4p$ dipole transitions. The energy position of the sharp and intense resonance A called the white line, is constant up to 130 °C (11107.6 eV), then from 136 °C it shifts to lower energy. Its energy position is 11107.1 eV at T = 154 °C. The post-edge features named A' (slope) and B (bump) are positioned only a few eV above A. The X-ray energy is then sufficient to excite electrons localized in shallow core levels with multi-electron processes. Multiple scattering paths around the excited atoms contribute strongly to the spectrum in the energy range of the C, C', and D features [26].

XANES is a very convenient experiment technique to discern the contribution of Ge–X (X = Te, Se) and Ge–O bonds in GeTe-based alloys due to a large shift in Ge K-edge X-ray absorption energy of about 7 eV between Ge–Te ($Ge^{+II}$) and Ge–O ($Ge^{+IV}$) bonds [27]. Our temperature-dependent Ge K-edge X-ray fluorescence experiments performed under an inert atmosphere did not point out the presence of the Ge-O bond contribution for our uncapped thick film samples in both the amorphous and the crystalline states. This confirms that uncapped GeTe films thicker than 50 nm are not affected by oxidation [23] even with the higher affinity of Ge to oxygen atoms than to the tellurium ones.

Figure 2(b) highlights the XANES differences between the amorphous and the crystalline state of the as-deposited GeTe thick film registered *in situ* with a continuous 0.2 °C/min heating rate. The intensity of the white line A becomes higher with the crystallization (even with the thermal damping), and both the A' slope and the D bump disappear. The Ge K-edge absorption threshold position $E_0$ (defines the onset of continuous states) and the white line *A* shift towards the lower energies when GeTe transits from an amorphous ($E_0$ = 11104.3 eV) to a crystallized ($E_0$ = 11103.7 eV) state, Figure 2(c). The shift in the $E_0$ values to lower energies is due to the decrease of the Coulomb interaction between the nuclear charge and the charge of the core electrons. Consequently, there is a more negative charge on the absorber and, thus, less energy

is required to excite an electron from an inner orbital. The whole changes are a clear indication of a local surroundings modification around the Ge atoms after the crystallization. The local order and electronic environment around Ge atoms are different between the amorphous and crystallized states of the GeTe phase change material.

In summary, the temperature-dependent XANES spectra recorded at the Ge threshold

i) discard the presence of $GeO_2$ contamination on the chalcogenide film surfaces,

ii) confirm the existence of the 3 zones (amorphous I, mix II, and crystalline III) shown by the XRD data,

iii) show a modification of the post-edge XANES features in energy and amplitude between the amorphous and the crystalline states due to structural and electronic evolution,

iiii) point out an evolution of the energy absorption threshold $E_0$ of Ge K-edge with the amorphous to crystalline transition.

### *3.2 $GeTe_{0.5}Se_{0.5}$ film*

#### *3.2.1 Temperature-dependent XRD patterns*

The chemical composition of the as-deposited 3-μm-thick Se-substituted GeTe film, amorphous in nature, is $Ge_{0.94}Te_{0.54}Se_{0.52}$ with an error estimated of ± 3 at.%. For simplicity's sake, the composition of this sample will be designed by $GeTe_{0.5}Se_{0.5}$. Figure 3 presents *in situ* synchrotron X-ray scattered intensity patterns recorded for this sample under an $N_2$ gas flux during continuous heating. Zone I corresponds to the amorphous state of the sample with a temperature of onset of crystallization of $T_c$ = 227 °C. In zone II, there is the coexistence of the two states, amorphous and crystalline, whose proportions change with temperatures. The high-temperature zone III starts at 278 °C, as shown by the presence of diffraction peaks only. The crystallization process, *i.e.*, when the degree of order in the material continues to increase,

is rather long for $GeTe_{0.5}Se_{0.5}$ film compared to the GeTe one, well above the onset crystallization temperature.

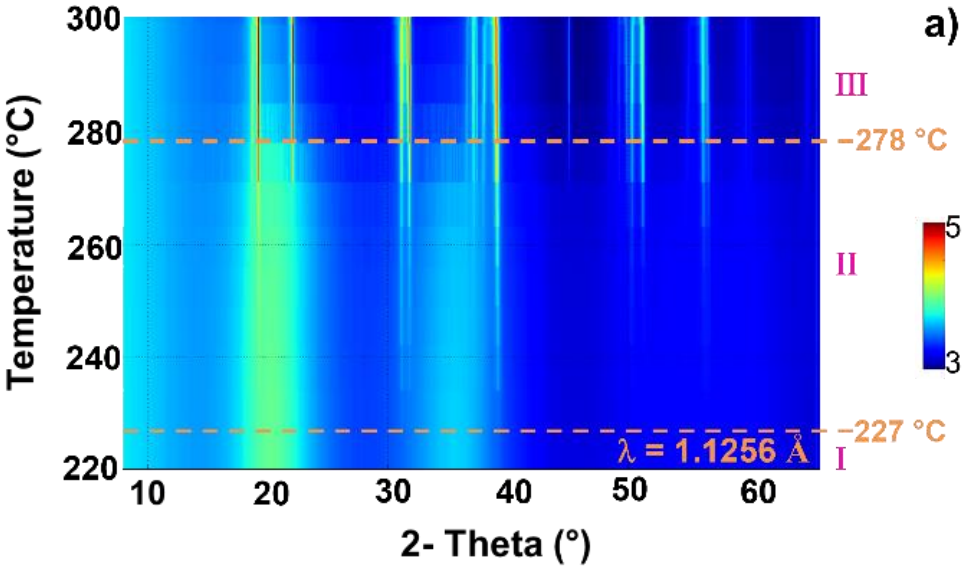


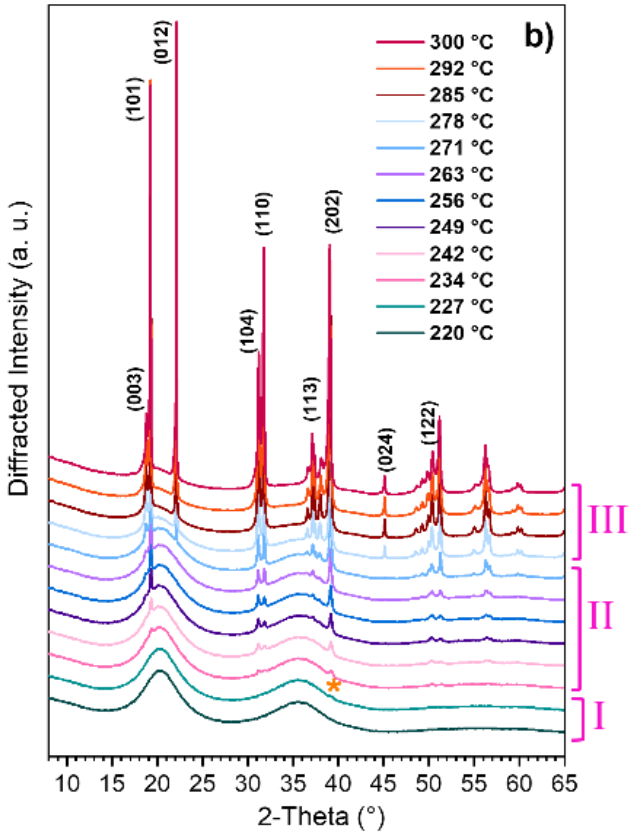


**Figure 3:** a) *In situ* temperature-dependent synchrotron X-ray scattering patterns registered on a $GeTe_{0.5}Se_{0.5}$ 3 µm-thick film deposited on a Si (001) substrate in isochronal annealing conditions (log scale in color), b) scattered intensity patterns at selected temperatures. The curves have been stacked

and vertically shifted for clarity. Only some main diffracted lines (in the hexagonal setting) are identified in the figure. The star pointed out the emergence of diffraction peaks at the onset temperature of crystallization $T_c$.

From 278 °C, all the diffracted lines are present and they are attributed to a rhombohedral space group *R*3*m* as for α-GeTe. The diffractograms show neither Ge, Te, or Se crystalline rejections nor secondary crystallized phases. Furthermore, with increasing temperature, we observe a shift in the opposite direction of the 2θ positions of the (003), (104), (101), and (110) diffraction peaks in the $GeTe_{0.5}Se_{0.5}$ rhombohedral structure, Figure 4, leading to the reduction of the $[2\theta_{101} - 2\theta_{003}]$ and $[2\theta_{110} - 2\theta_{104}]$ differences.

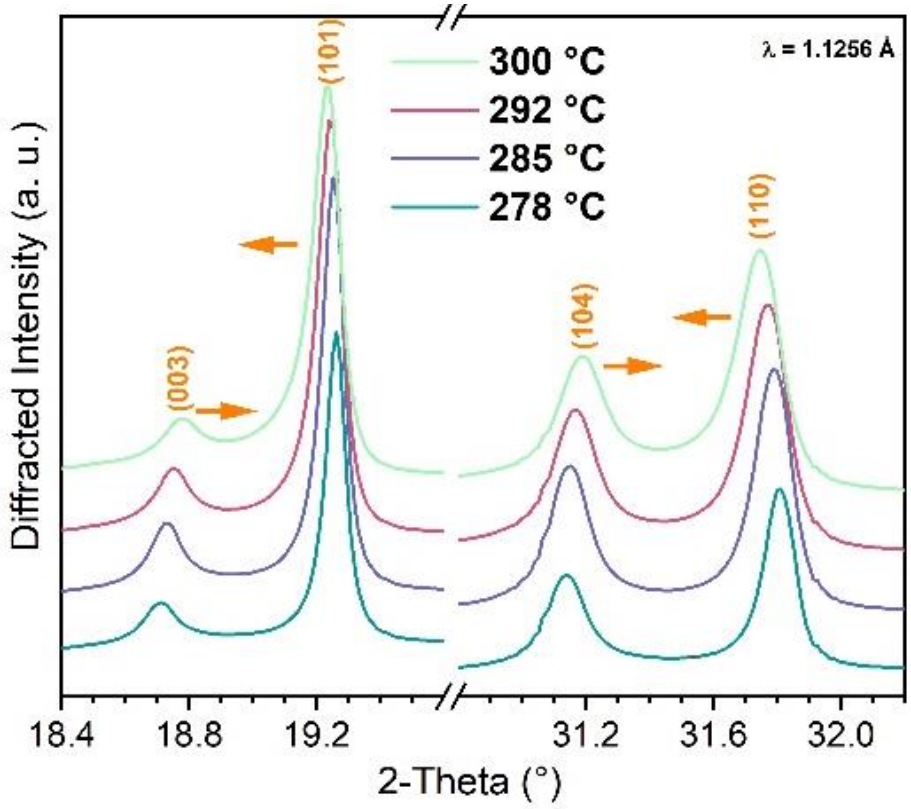


**Figure 4:** Graphical highlight of the diminution of the $[2\theta_{101} - 2\theta_{003}]$ and $[2\theta_{110} - 2\theta_{104}]$ differences with the heating temperature (from bottom to top) of the α-$GeTe_{0.5}Se_{0.5}$ structure. The shift in 2θ position (for the various Bragg peaks) with the temperature increasing is shown by arrows. The curves are shown vertically shifted for better visibility.

Compared to the α-GeTe parent film, the diffraction peaks of the Se-doped film are sharper, indicating a better crystallinity of the Se-substituted film with an increase in the average crystalline domain size as shown in Table IV. We note a decrease in the average crystallite size with the higher temperatures instead of an augmentation as expected. This is due to the increase of the thermal disorder with high temperatures with, as a consequence, an enlargement of the width of the diffraction peaks which is not taken into account in Debye-Scherrer's law.

**Table IV:** Temperature-dependent half-angle position of the (012) main XRD peak obtained on the α-$GeTe_{0.5}Se_{0.5}$ thick film with a wavelength λ of 1.1256 Å, its FWHM, and the calculated *D* parameters. The instrument resolution function (~ 0.02 - 0.03° in 2-theta) was not deconvoluted from the measurements. The incertitudes are given in parentheses.

| **T (°C)** | **θ (°) (012) peak** | **FWHM (rad) (012) peak** | ***D* (nm)** |
|---|---|---|---|
| **278** | 11.06(1) | 0.0012(4) | 81.93(1) |
| **285** | 11.06(1) | 0.0012(4) | 81.93(1) |
| **292** | 11.05(1) | 0.0015(4) | 65.55(1) |
| **300** | 11.05(1) | 0.0018(4) | 56.71(1) |

Again, the temperature-dependent *a* and *c* cell parameters were calculated with the help of the $d_{110}$ and the $d_{104}$ interplanar distances obtained at selected temperatures (Eqs.(1)-(2)), and are reported in Table V. The results pointed out cell parameter changes due to thermal expansion and deformation with increasing temperature. We notice the anisotropy of the thermal

expansion, with a positive coefficient of expansion following the *a* cell parameter, while that following *c* is negative, and consequently a diminution of the *c*/*a* ratio.

**Table V:** Temperature-dependent half-angle (θ) positions (on continuing heating) of two selected diffracted peaks obtained with a wavelength λ of 1.1256 Å on the α-$GeTe_{0.5}Se_{0.5}$ film, with the corresponding inter-planar distances $d_{hkl}$, the *c*, and *a* cell parameters, the *c*/*a* ratio, and the cell volume *V*. The incertitudes are given in parentheses.

| **T°** | **278 °C** | | | **285 °C** | | | **292 °C** | | | **300 °C** | | |
|---|---|---|---|---|---|---|---|---|---|---|---|---|
| **(*hkl*)** | **θ (°)** | **$d_{hkl}$ (Å)** | ***c*, *a* (Å)** | **θ (°)** | **$d_{hkl}$ (Å)** | ***c*, *a* (Å)** | **θ (°)** | **$d_{hkl}$ (Å)** | ***c*, *a* (Å)** | **θ (°)** | **$d_{hkl}$ (Å)** | ***c*, *a* (Å)** |
| **(*104*)** | 15.57(1) | 2.10(4) | 10.38(8) (*c*) | 15.58(1) | 2.09(4) | 10.37(8) (*c*) | 15.59(1) | 2.09(4) | 10.35(8) (*c*) | 15.60(1) | 2.09(4) | 10.34(8) (*c*) |
| **(*110*)** | 15.91(1) | 2.05(4) | 4.11(8) (*a*) | 15.91(1) | 2.05(4) | 4.11(8) (*a*) | 15.89(1) | 2.05(4) | 4.11(8) (*a*) | 15.87(1) | 2.058(4) | 4.12(8) (*a*) |
| ***V* (Å³)** | 151.7(2) | | | 151.5(2) | | | 151.5(2) | | | 151.7(2) | | |
| ***c* / *a*** | 2.53 | | | 2.52 | | | 2.52 | | | 2.51 | | |

### *3.2.2 Temperature-dependent XANES spectra*

Simultaneously with the temperature-dependent XRD data collection on heating, the fluorescence-detected XANES signals of the as-deposited $GeTe_{0.5}Se_{0.5}$ thick film were collected around the Ge and Se K-edges, with the isochronal annealing conditions.

Figure 5(a) presents a selection of Ge K-edge XANES spectra compared with the XANES curve of the crystalline bulk reference α-$GeTe_{0.5}Se_{0.5}$ (space group *R*3*m*) contained in a capillary tube and measured at 25 °C. Three distinctive general shapes of the XANES spectra are visible depending on the registered temperature. The first one, from 220 to 249 °C, characterizes

mainly the amorphous state with the A white line and the slope A'. The second spectral shape, from 256 °C to 271 °C, with A and a weak, broad bump, is due to the mixing of the amorphous and the crystalline states (see zone II in Figure 3) whose proportion depends on the temperature. The third distinctive shape, from 278 to 300 °C, is due to the rhombohedral structure with line A, a weak B bump, and a C feature located at larger energy. As for the undoped GeTe film, no Ge-O XANES feature is detected whatever the temperature, indicating the lack of a $GeO_2$ layer on the surface of the $GeTe_{0.5}Se_{0.5}$ uncapped film.

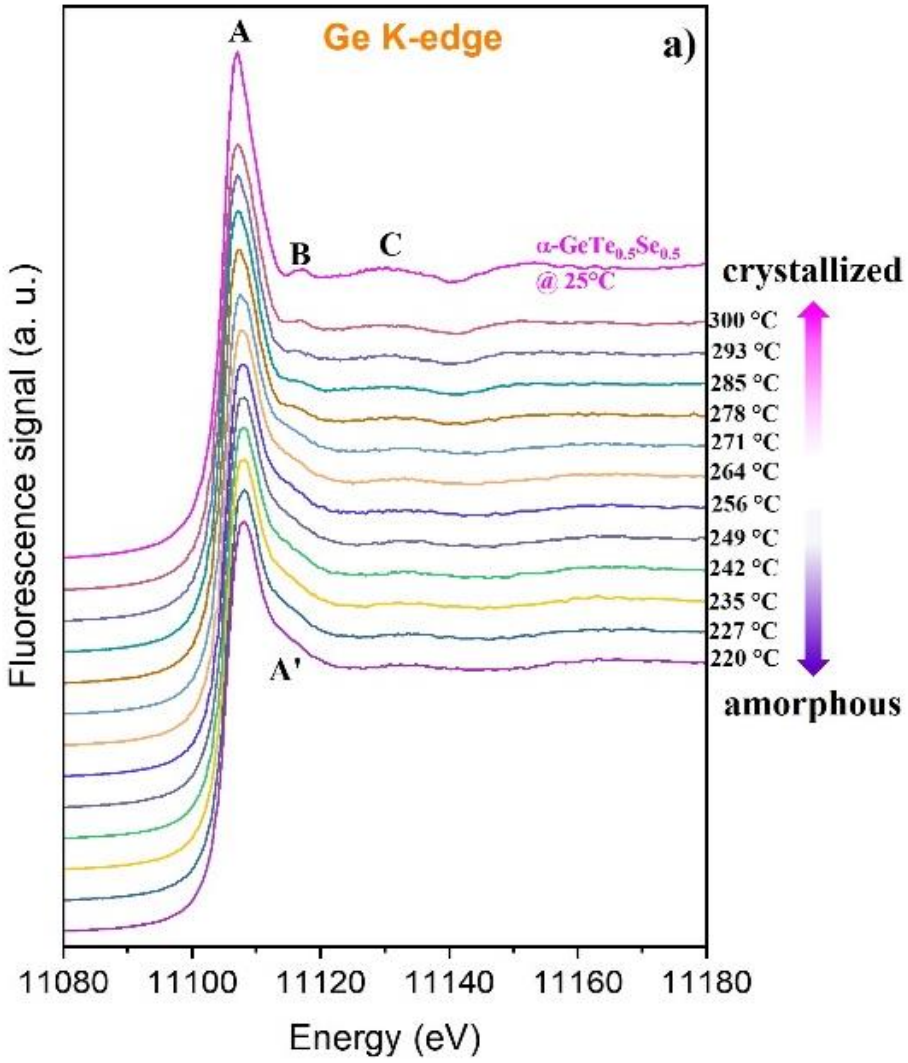

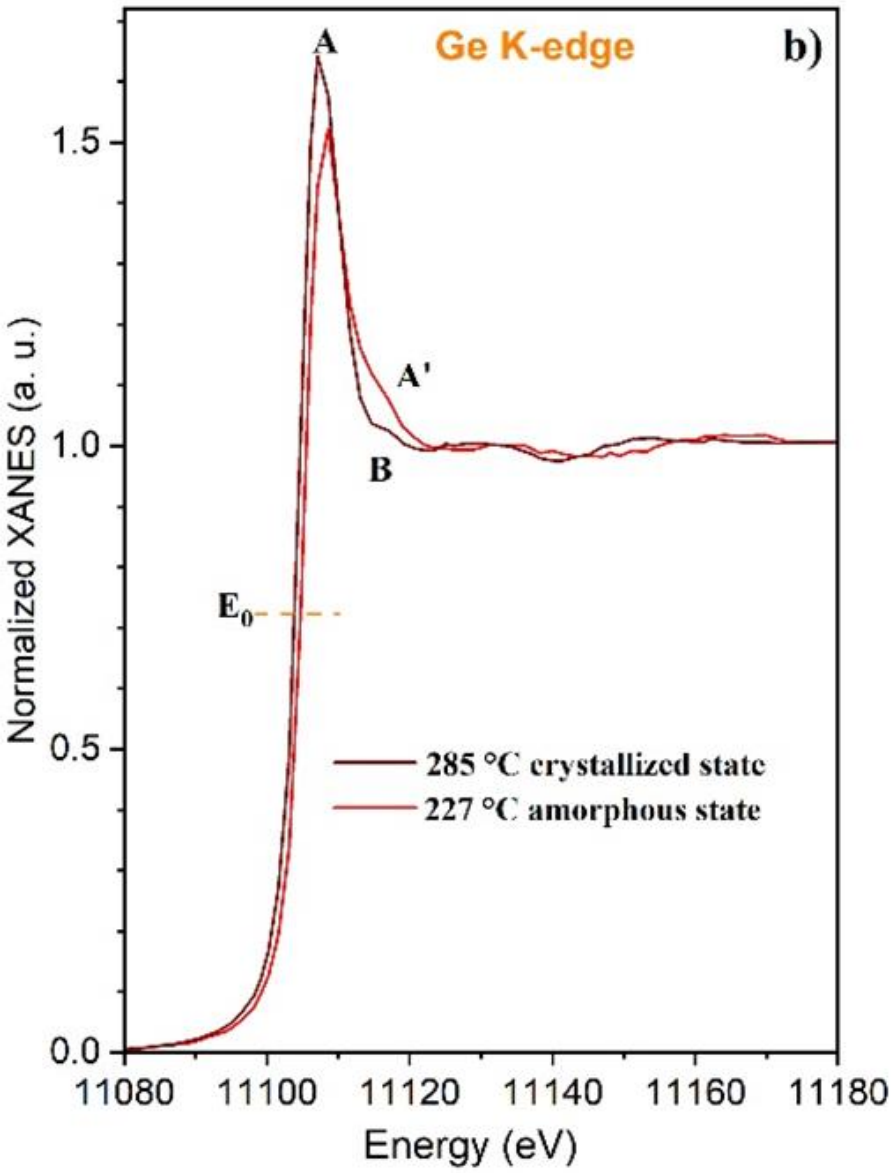


**Figure 5:** a) Evolution with the heating temperature of the Ge K-edge near-edge features in the fluorescence-detected XANES spectra of the as-deposited $GeTe_{0.5}Se_{0.5}$ thick film compared to that of the powdered crystalline reference $\alpha$-$GeTe_{0.5}Se_{0.5}$ (*R*3*m*) registered at ambient conditions (pink curve). The spectra are presented as collected and have been stacked and vertically shifted for clarity. b) comparison of the normalized XANES spectra taken in the amorphous (zone I of Figure 3) and crystallized (zone III of Figure 3) states.

Figure 5(b) highlights the differences in the XANES features between the amorphous and the crystalline states of the $GeTe_{0.5}Se_{0.5}$ film. As for the undoped GeTe film, the Ge K-edge absorption threshold position $E_0$, and the white line *A* shift towards the lower energies when the

sample transits from an amorphous to a crystallized state. This is a clear indication of a local surroundings modification around the Ge atoms after the crystallization.

Figure 6(a) presents a selection of Se K-edge XANES spectra of the Se-substituted GeTe film compared with the XANES curve of the bulk crystalline α-$GeTe_{0.5}Se_{0.5}$ registered at 25 °C. The ground state electronic configuration of the atomic Se is [*Ar*] $3d^{10}4s^24p^4$ and its atomic outer shell electronic configuration is $4s^24p_x^1p_y^1p_z^2$ [11]. In the band structure approach, Se K-edge XANES probes the final unoccupied partial density of states with dominant *p*-like symmetry, and the absorbing edge, the allowed dipole transition from the Se 1*s* core state to the "4*p* (Se)" empty final state.

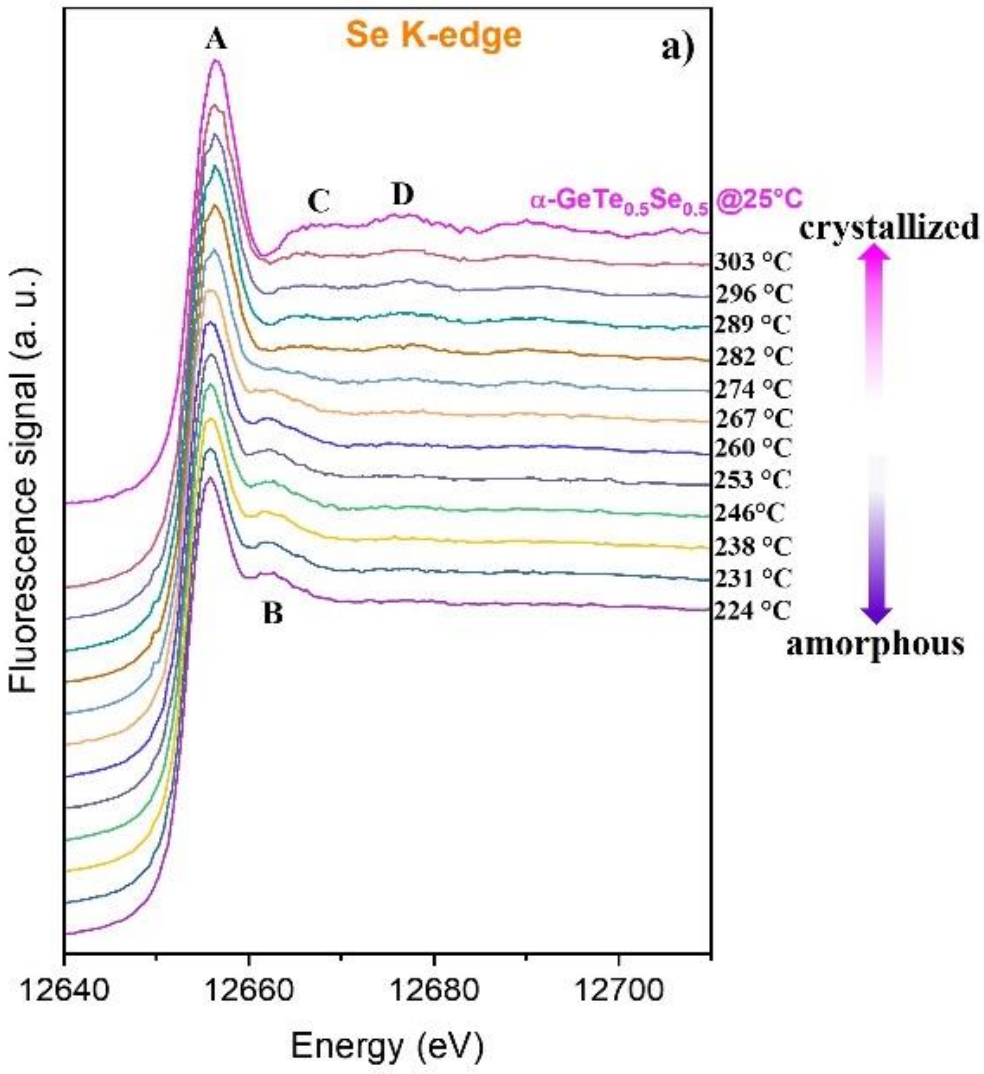

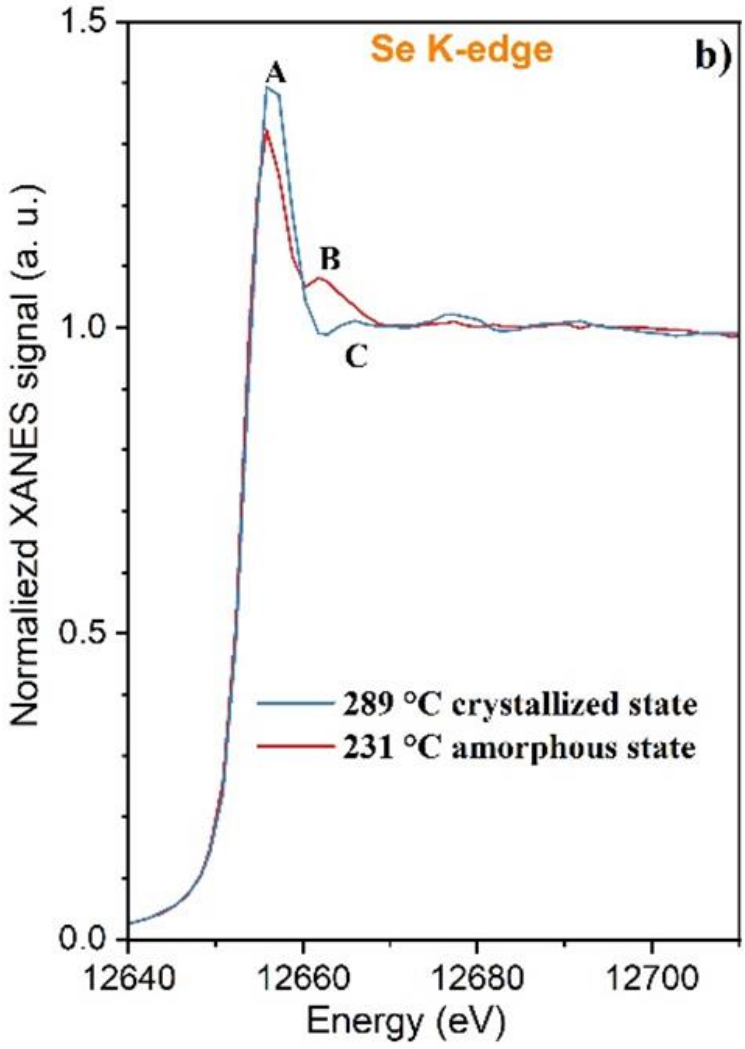


**Figure 6:** a) Evolution with the heating temperature of the Se K-edge near-edge features in the fluorescence-detected XANES spectra of the as-deposited $GeTe_{0.5}Se_{0.5}$ thick film compared to that of the powdered (bulk) crystalline reference α-$GeTe_{0.5}Se_{0.5}$ (*R*3*m*) registered at ambient conditions. The spectra have been vertically shifted for clarity. b) comparison of the normalized XANES spectra taken in the amorphous (zone I of Figure 3) and crystallized (zone III of Figure 3) states.

Three distinctive general shapes of the experimental Se K-edge XANES spectra are visible in Figure 6(a), even if a sharp rise in absorption is observed for all of them. From 224 °C to 267 °C, the XANES spectra present a white line A and a B broad hump, which are mainly the signature of the local structure of the Se shell in the amorphous $GeTe_{0.5}Se_{0.5}$. The spectrum registered at 274 °C constitutes the second general shape, the B bump is no longer present, and

the distant D feature is just starting to appear. The third shape goes from 282 °C to 303 °C with the apparition of the C and D bumps driven by the multiple-scattering of the photoelectron with the nearest neighbors. In this temperature range, the rhombohedral structure of $GeTe_{0.5}Se_{0.5}$ is the main phase present as shown by the XRD analysis, zone III in Figure 3. This is confirmed by the close resemblance of the XANES spectra with the one of the crystallized α-$GeTe_{0.5}Se_{0.5}$ used as a bulk reference (registered at 25 °C).

A significant intensity augmentation of the white line A is observed with heating, suggesting an increased number of Se 4*p*-like unoccupied DOS in the conduction band, Figure 6(b). The evolution of both the *p*-like density of states and the multiple scattering humps (B, C, D) from the amorphous to the crystallized states could be related to changes in the local geometry around the Se atoms even if the variation of the $E_0$ position during the whole experiment is not significative.

The non-qualitative XANES study provides interesting information on the Se doping effect in GeTe parent film in the amorphous and the crystalline states which is the augmentation of the short-range disorder brought mainly by bond lengths and angles spread. This information is not accessible with the XRD data. On the contrary, XRD data concerning the long-range order show that the crystallinity of the Se-doped GeTe film is better with the existence of larger grain domains. The structural information brought by the two characterization techniques is complementary.

## 4. Discussion

The primitive cell of α-GeTe is characterized by a polar distortion where the Ge and Te atoms are displaced from the high symmetry position of (0,0,0) and (1/2,1/2,1/2), respectively along the [111] crystallographic direction. The rhombohedral layered α-GeTe crystalline structure has

short bonds at 2.83 Å and long interactions at 3.16 Å [13] and can accommodate the smaller Se atoms [11, 13, 17].

The cell parameters evaluations (*a* and *c* in the hexagonal description of the rhombohedral lattice) of GeTe and the $GeTe_{0.5}Se_{0.5}$ solid solution, in the function of the temperature, see Tables III and V, show a decrease with the Te partial substitution by Se, in agreement with the smaller size of Se (119 pm) compared to the giant Te (142 pm). Indeed, the formation of more covalent and stronger Ge–Se bonds to the detriment of weaker metavalent Ge–Te bonds in α-$GeTe_{0.5}Se_{0.5}$ alloy increases the rigidity of its structural network compared to α-GeTe. Moreover, the absence of a crystallized Se-based parasitic phase on the X-ray diffraction patterns of the $GeTe_{0.5}Se_{0.5}$ solid solution, Figure 3, favors a total substitution of Te by Se into the GeTe rhombohedral lattice. This result confirms the large solubility of GeSe in GeTe [13]. The α-$GeTe_{0.5}Se_{0.5}$ material is then isostructural of α-GeTe [13]. Se atoms substitute 50 % of the Te atoms, meaning that the anion sites are occupied by Te/Se and the cation sites by $Ge^{II}$. Se and Te atoms are also [3+3]-fold coordinated but form heteropolar bonds (short and long bonds) only with Ge atoms.

The thermal evolution of the lattice parameters pointed out, for the two samples in this study, a negative thermal expansion (NTE) along the *c*-axis, while the $a = b$ cell parameters have a positive thermal expansion for the ternary alloy, and they stay rather constant for α-GeTe, Tables III and V. An NTE phenomenon (also known as "contraction upon heating") in one crystallographic direction, here *c* in the hexagonal cell, was already reported for the $GeTe_{0.26}Se_{0.74}$ rhombohedral structure [22]. Consequently, the *c*/*a* ratios present a negative thermal-dependent evolution on heating, Tables III and V. Moreover, the deviation of their values from the ideal *c*/*a* ratio value ($\sqrt{6} \sim 2.4495$), derived from the description of an ideal face-centered cubic cell of a primitive rhombohedral-centered cell in the hexagonal setting ($Fm\bar{3}m$) [8], is reduced with the heating. This is due to the existence of a rhombohedral to cubic

($R3m \rightarrow Fm\bar{3}m$) transformation announced in the pseudo-binary GeTe-GeSe [16] to occur at 370 ± 10 °C for $GeTe_{1-x}Se_x$ compositions with $0 \leq x \leq 0.55$. Thus, increasing the temperature allows the diminution of the rhombohedral cell distortion by reducing the displacements of Ge and Te atoms from the high symmetry position of (0,0,0) and (1/2,1/2,1/2) in the primitive cell and by approaching the ideal rhombohedral interaxial angle of 60°. This is also pointed out by the reduction of the peak position difference $[2\theta_{110} - 2\theta_{104}]$ in α-$GeTe_{0.5}Se_{0.5}$ with the heating, Figure 4. Indeed, in the fcc rock salt structure, the (104)-(110) XRD peaks in *R*3*m* collapse in a (220) one.

No indication of individual element segregation and crystallization or parasitic phases was found in the crystallized state of the two alloys under study whatever the recorded temperature. By replacing 50 at. % of Te by Se into the α-GeTe parent, the intensity of the whole XRD peaks in zone III (rhombohedral structure) increases significantly compared to the undoped GeTe material, Figures 1 and 3. This may be because the temperatures of the crystallized domain registered here for the ternary alloy ($278 < T \leq 300$ °C) are well above the ones for α-GeTe ($136 \leq T \leq 154$ °C) which then increases the average size of the crystallites as shown in Table IV.

The onset temperature of crystallization $T_c$ is 124 °C for the uncapped 3 μm thick GeTe film heated under a nitrogen-protective atmosphere. A temperature of crystallization of 129 °C is also reported for a 1 μm thick uncapped GeTe film heated in He atmosphere [28] while $210 \leq T_c \leq 240$ °C is found for the crystallization of GeTe nanoparticles under nitrogen flow [29]. A $T_c$ of 235 °C is measured on 100 nm GeTe films deposited on Si(001), capped by a 10 nm TaN protective layer, annealed *in situ* under $N_2$ [8, 30]. It is reported that $T_c$ values under 200 °C for GeTe films would be the consequence of surface oxidation [8, 30]. Concerning this work, the XANES data confirms the lack (within the detection limit) of oxidation on the surface of our

samples *i.e.*, the formation of a $GeO_2$ layer. X-ray absorption spectroscopy is strongly surface sensitive especially when the grazing technique is applied as in our experiments [31]. Measurements with the fluorescence mode can be made on elements of minority and even trace abundance. Thus, for non-oxidized GeTe amorphous samples, the large temperature domain reported for their crystallization temperature may be the consequence of other factors such as the film thickness, the preparation technique, the substrate, the chemical composition (stoichiometry or not), the nature of defects, the atomic arrangement in the amorphous state, the heating rate, the annealing threshold, and so on [22].

The onset temperature of crystallization significantly increases with the Se-substitution going from 124 °C for α-GeTe to 227 °C for α-$GeTe_{0.5}Se_{0.5}$. These results are in good agreement with a previous temperature-dependent synchrotron X-ray diffraction study on an uncapped $GeTe_{0.26}Se_{0.74}$ 3-μm thick film obtained by thermal co-evaporation where the appearance of the rhombohedral diffraction peaks ($T_c$) was observed at 249 °C for the same heating rate (0.2 °C/min) [22]. The augmentation of $T_c$ with the Te/Se substitution is an indication of the amorphous state stability, owing to the easy glass formability of the Se, which, for a phase change material, could allow higher operating temperatures. Furthermore, we noticed a larger domain of existence of zone II in the XRD results of the doped alloy (Figure 3) related to the mixing of the amorphous state (zone I) and crystallized state (zone III) whose proportion depends on the temperature. This means that a wider range of temperatures is required for the thermal energy to cause the entire amorphous phase to switch to the crystallized phase when 50 at. % of Te atoms are replaced by Se.

For both GeTe parent and $GeTe_{0.5}Se_{0.5}$ thick films, significant differences in the shape and intensities of the Ge and Se K-edge absorption curves are visible between the amorphous and the crystallized states emphasizing local order modifications around the probed atoms (Figures 2, 5, and 6). Moreover, differences are visible on the normalized Ge K-edge XANES spectra

between the GeTe material and the Se-substituted GeTe one in both states, Figure 7, but they are more pronounced in the crystalline state, Figure 7(b).

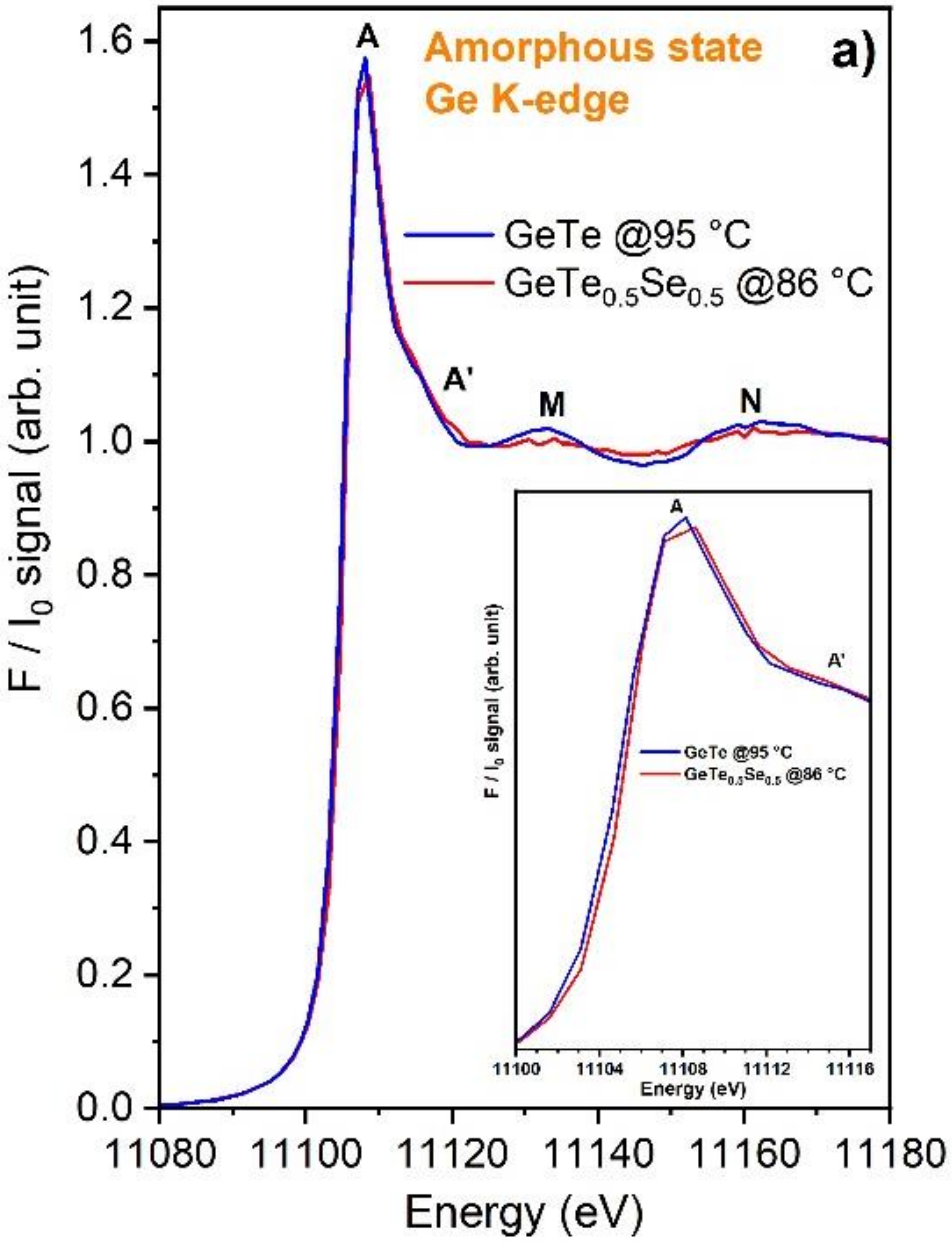

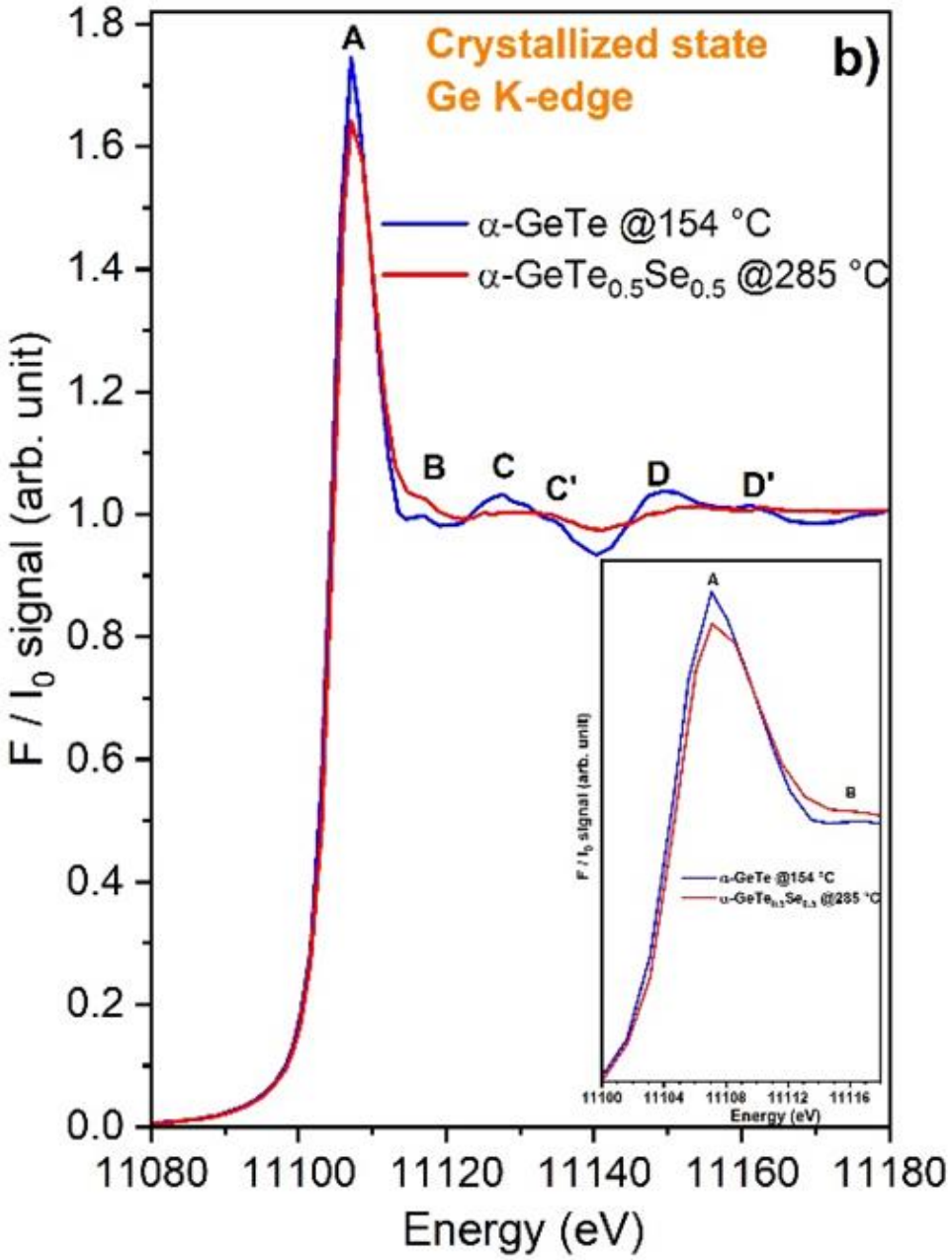


**Figure 7:** Normalized Ge K-edge spectra for the GeTe and $GeTe_{0.5}Se_{0.5}$ films recorded in a) the amorphous state and b) the crystalline state. The inserts emphasize the white line position and amplitude.

In the amorphous state, the general appearance of the XANES curves presents close similitude between GeTe and the ternary composition, especially concerning the A and A' features, Figure 7(a). Amorphous materials present short-range order, and so, we may expect a similar local

symmetry in both amorphous samples with a close number of available unoccupied states for the transition from the Ge 1*s* states. The Se-substitution mainly affects the widths and the energy position of the humps M and N, Figure 7(a). The apparent broadening in the multiple scattering range of the $GeTe_{0.5}Se_{0.5}$ film compared to the GeTe one is mainly due to the formation of the Ge-Se heteropolar bonds also responsible for the difference in the binding energy $E_0$ position, which is 11104.7 eV for GeTe and 11105.00 eV for $GeTe_{0.5}Se_{0.5}$, see the insert in Figure 7(a). Owing to the higher electronegativity of Se (Se (2.55) and Te (2.1) on the Pauling scale), higher energy Ge–Se bonds (2.14 eV) are formed at the expense of low energy Ge–Te bonds (1.53 eV) [13].

Published room-temperature Ge K-edge experimental XANES spectra of amorphous, as-deposited 50 nm thick $Ge_xTe_{1-x}$ films ($x$ = 0.5, 0.6, 0.7) [20] present a general spectral shape comparable to our temperature-dependent spectra collected in the amorphous state. A very close similitude is obtained for the binary composition with $x$ = 0.5. Their *ab initio* full multiple scattering simulations are consistent with the existence of 4(Ge)-coordination number to reproduce the A white line, the A' slope, and the D bump. Tetrahedral local order around Ge atoms was reported for amorphous $GeTe_{1-x}Se_x$ 6 μm thick films ($x$ = 0, 0.5, 0.75, 1) investigated by combining the room temperature X-ray total scattering and density functional-based molecular dynamics [32]. A step-like feature at the Ge $L_3$-edge absorption edge, corresponding to a Ge $2p \rightarrow 5s$ ($4d$) electron transition, appears for amorphous GeTe-based films. The *ab initio* XANES simulations suggest that the step-like feature is due to the existence of tetrahedrally coordinated Ge atoms in the as-deposited samples [33]. The presence of corner-sharing $GeTe_4$ was also identified in Ge-poor $Ge_xTe_{100-x}$ glasses ($x$ = 14.5, 18.7, 23.6) by the reverse Monte Carlo simulations of neutron diffraction, X-ray scattering, and Ge K-edge EXAFS data [34].

Figure 7(b) emphasizes, in the crystallized state, the structural and electronic differences between α-GeTe and Se-substituted (50 at. %) α-GeTe film samples at the Ge K-edge. The

XANES features are better defined for α-GeTe compared to the substituted film. This could be explained by the *in situ* registered temperature difference, higher for α-$GeTe_{0.5}Se_{0.5}$ (285 °C) than α-GeTe (154 °C), and by the local structural disorder differences around the Ge atoms between the two compositions. Indeed, both the dynamic (thermal agitation) and the static contributions (variation of the distribution of distances between absorbing and backscattering atoms [35]) of the Debye-Waller factor DWF (temperature factor) exponentially damped the X-ray absorption signal at high temperatures. With the Se-substitution of Te atoms in α-GeTe, a higher degree of disorder in the first solvation shell around Ge atoms is expected with the existence of metavalent Ge-Te and covalent Ge-Se bonds having different bong lengths and thus, with a broader *X*-Ge-*X* (*X* = Te, Se) angle distribution compared to α-GeTe. Ge K-edge X-ray fluorescence spectrum is sensitive to the local disorder in the Te/Se sub-lattice.

As already shown, the electronic and the Ge surroundings in the two chalcogenide films under study undergo a major modification upon crystallization as their XANES spectra present clear differences between the amorphous and the crystallized states, Figure 7. A material is defined by its atomic coordination number, which is linked to its bonding nature. This relationship has a profound influence on the resultant electronic band structure which, in turn, governs numerous properties exhibited by functional materials. The 4-fold coordination of the Ge atoms in these amorphous GeTe-based covalent solids is well established in the literature [20, 32, 33, 34, 36], while a [3+3]-fold coordination (3 shorts at ~2.84 Å + 3 longs at ~3.15 Å) is present in the rhombohedral structure with metavalent bonding. The four-fold (covalent)-to-six-fold coordination (metavalent) transformation upon crystallization affects the Ge K-edge XANES spectra which are the fingerprints of the local atomic and electronic structures around the absorbing atom.

Comparing both GeTe-based systems in their crystalline state from their X-ray diffraction patterns, which are mainly sensitive to the long-range order, Figures 1 and 3, we noticed that

the main effect of the Se doping of the GeTe parent film is in narrower Bragg peaks with larger diffraction domains, Tables II and IV. The effect of the Se/Te random substitution would enlarge the sample crystallinity. On the opposite, as XANES is extremely sensitive to local order/disorder around the probed atom, we noticed a different effect of the random substitution of Te by Se on the features. In this case, the Ge first coordination shell in the Se substituted GeTe film is associated to a smoother profile resulting in a higher local disorder than in GeTe polycrystalline film, Figure 7(b). This disorder is mainly due to greater length and angle distributions with the formation of Ge-Te and Ge-Se bonds. The structural information brought by the two characterization techniques is complementary.

## 5. Conclusions

In this work, we have investigated the effect of the substitution of 50 at. % of Te atoms by Se ones in unencapsulated GeTe thick film on the phase change behavior via *in situ* temperature-dependent loops, recorded continuously (no step) with a 0.2 °C/min, of XR scattering measurements, coupled with XANES measurements. These two characterization techniques are complementary, XRS is sensitive to the long range order while XANES is a more local order probe.

As for GeTe film, the doped alloy crystallizes in the rhombohedral structure, with no phase separation and without Ge or Te rejection, but at higher temperatures and with less long-range structural distortions. The lack of Se-based crystallized parasitic phases and the registered decrease of the unit cell parameters for the Se-substituted GeTe film confirmed the incorporation of Se in the structure. Some effects of the Te/Se substitution in the base GeTe material were pointed out, as, a great increase in the value of the onset of crystallization $T_c$ ($\Delta T_c$ ~ 100 °C), and a larger temperature range of the coexistence of the amorphous /crystalline state,

due to the more covalent character of selenium and then, to a more rigid ternary network. Thus, achieving a complete amorphous to crystalline state transition (switching) would necessitate more thermal energy for the doped GeTe film and/or a higher switching duration time (speed) than for GeTe. Therefore, a higher crystallization temperature is required for the stable operation of the memory cells and a large amorphous range is important for data retention when information needs to be stored for a long time at elevated temperature.

The Te/Se substitution affects also the local and medium-range order around the Ge atoms and the Ge empty-DOS. The formation of two types of heteropolar bonds with different lengths, covalent Ge-Se and metavalent Ge-Te, raises the local distortion of the Ge shell which is reflected on the Ge K-edge XANES spectra as their amplitude oscillations are influenced by the local disorder of thermal and static origin.

The Ge K-edge fluorescence-type XANES study has shown a close local order and electronic configuration in the amorphous state between the two compositions under study related to the existence of Ge 4-fold coordinated. A clear evolution of the Ge and Se K-edge XANES spectra was recorded between the amorphous and the crystalline phases for both GeTe and $GeTe_{0.5}Se_{0.5}$ films. This feature evolution is attributed to a modification of the Ge and Se first shells from the amorphous (Ge 4-fold and Se 2-fold) to the crystalline state (Ge and Se [3+3]-fold coordinated) in perfect accordance with their phase change behavior.

**Funding:** This work was supported by the French Ministry of Higher Education, Scientific Research and Innovation, and the French National Center of Scientific Research (CNRS).

**Acknowledgments:** EDX measurements were done at the Platform of Analysis and Characterization (PAC) of the Pôle Chimie Balard in Montpellier, France. The *in-situ* temperature-dependent experiments (proposal ID 20210201) were performed at Synchrotron SOLEIL facility (France) on the DiffAbs beamline. P. Joly (DiffAbs beamline) is acknowledged for technical support during the experiments.

**References:**


[1] Wide range optical and electrical contrast modulation by laser-induced phase transitions in GeTe thin films
N. N. Eliseev, A. V. Kiselev, V. V. Ionin, V. A. Mikhalevsky, A. A. Burtsev, M. A. Pankov, D. N. Karimov, A. A. Lotin
Results in Physics 19 (2020) 103466
https://doi.org/10.1016/j.rinp.2020.103466

[2] Metavalent Bonding in Crystalline Solids: How Does It Collapse?
L. Guarneri, S. Jakobs, A. von Hoegen, S. Maier, M. Xu, M. Zhu, S. Wahl, C. Teichrib, Y. Zhou, O. Cojocaru-Mirédin, M. Raghuwanshi, C.-F. Schön, M. Drögeler, C. Stampfer, R. P. S. M. Lobo, A. Piarristeguy, A. Pradel, J.-Y. Raty, Matthias Wuttig
Adv. Mater. 33 (2021) 2102356
https://doi.org/10.1002/adma.202102356

[3] Evolution of the Structural and Electrical Properties of GeTe Under Different Annealing Conditions
K.-H. Kim, Y.-K. Kyoung, J.-H. Lee, Y.-N. Ham, S.-J. Choi
J. Electronic Materials 42 (2013) 78–82.
https://doi.org/10.1007/s11664-012-2262-8

[4] Evolution of crystal structures in GeTe during phase transition
K. Jeong, S. Park, D. Park, M.Ahn, J. Han, W. Yang, H.-S. Jeong, M.-H. Cho
Sci. Rep. 7 (2017) 955
https://doi.org/10.1038/s41598-017-01154-z

[5] Incipient metals: functional materials with a unique bonding mechanism
M. Wuttig, V. L. Deringer, X. Gonze, C. Bichara, J.-Y. Raty,
Adv. Mater. 30(51) (2018) 1803777.
https://doi.org/10.1002/adma.201803777

[6] A Quantum-Mechanical Map for Bonding and Properties in Solids
J.-Y. Raty, M. Schumacher, P. Golub, V. L. Deringer, C. Gatti, M. Wuttig
Adv. Mater. 31 (2019) 1806280
https://doi.org/10.1002/adma.201806280

[7] Metavalent Bonding in Solids: Characteristic Representatives, Their Properties, and Design Options
Y. Cheng, S. Wahl, M. Wuttig
Phys. Status Solidi RRL 15 (2021) 2000482
https://doi.org/10.1002/pssr.202000482

[8] New insights into thermomechanical behavior of GeTe thin film during crystallization
M. Gallard, M. Salah Amara, M. Putero, N. Burle, C. Guichet, S. Escoubas, M.-I. Richard, C. Mocuta, R. R. Chahine, M. Bernard, P. Kowalczyk, P. Noé, O. Thomas.
Acta Materialia 191 (2020) 60 – 69.
https://doi.org/10.1016/j.actamat.2020.04.001

[9] Crystallization of GeTe phase change thin films grown by pulsed electron-beam deposition
N. Bathaei, B. Weng, H. Sigmarsson
Mater. Sci. Semicond. Process. 148 (2022) 106781
https://doi.org/10.1016/j.mssp.2022.106781

[10] In situ monitoring of stress change in GeTe thin films during thermal annealing and crystallization
B. Ben Yahia, M.S. Amara , M. Gallard, N. Burle, S. Escoubas , C. Guichet , M. Putero , C. Mocuta, M.-I. Richard, R. Chahine, C. Sabbione, M. Bernard, L. Fellouh, P. Noé, O. Thomas.
Micro Nano Engi. 1 (2018) 63 – 67.
https://doi.org/10.1016/j.mne.2018.10.001

[11] Electrical switching properties and structural characteristics of GeSe–GeTe films
K. Ren, M. Zhu, W. Song, S. Lv, M. Xia, Y. Wang, Y. Lu, Z. Jib, Z. Song
Nanoscale 11 (2019) 1595–1603.
https://doi.org/10.1039/C8NR07832G

[12] Overcoming the Thermal Stability Limit of Chalcogenide Phase-Change Materials for High-Temperature Applications in $GeSe_{1-x}Te_x$ Thin Films
M. Tomelleri, F. Hippert, T. Farjot, C. Licitra, N. Vaxelaire, J.-B. Dory, D. Benoit, V. Giordano, P. NoéPhys. Status Solidi RRL 15 (2021) 2000451
https://doi.org/10.1002/pssr.202000451

[13] Structural transformation and phase change properties of Se substituted GeTe
R. Shekhawat, H. Pamuluri, V. Erkkara Madhavan, K. Ramesh
Sci. Rep. 11 (2021) 7604
https://doi.org/10.1038/s41598-021-87206-x

[14] Effect of selenium addition on the GeTe phase change memory alloys
E.M. Vinod, A.K. Singh, R. Ganesan, K.S. Sangun
J. Alloys and Compounds 537 (2012) 127–132
http://dx.doi.org/10.1016/j.jallcom.2012.05.064

[15] The effect of Se doping on spectroscopic and electrical properties of GeTe
E. M. Vinod, K. S. Sangunni
Thin Solid Films 550 (2014) 569–574
http://dx.doi.org/10.1016/j.tsf.2013.11.038

[16] Phase transformations in the system GeSe-GeTe.
J. A. Muir, V. Beato
J. Less Common Metals 33(3) (1973) 333–340.
https://doi.org/10.1016/0022-5088(73)90185-9

[17] The Temperature-Composition Phase Diagram of the GeSe-GeTe System
H. Wiedemeier, P. A. Siemers
Edited in book Modern High Temperature Science, pp 395 – 40 (1984). Editor: John L. Margrave Publisher: Humana Totowa, NJ
https://doi.org/10.1007/978-1-4612-5180-4

[18] Structure-Dependent Thermoelectric Properties of $GeSe_{1-x}Te_x$ ($0 \leq x \leq 0.5$)
Z. Wang, H. Wu, Ming Xi, H. Zhu, Lu Dai, Q. Xiong, G. Wang, G. Han, X. Lu, X. Zhou, G. Wang
ACS Appl. Mater. Interfaces 12 (2020) 41381–41389
https://doi.org/10.1021/acsami.0c10850

[19] Towards accurate models for amorphous GeTe: crucial effect of dispersive Van der Waals corrections on the structural properties involved in the phase change mechanism
M. Micoulaut, A.A. Piarristeguy, H. Flores-Ruiz, A. Pradel
Phys. Rev. B 96 (2017) 184204
https://doi.org/10.1103/PhysRevB.96.184204

[20] Structural analyses of phase stability in amorphous and partially crystallized Ge-Rich GeTe films prepared by atomic layer deposition
T. Gwon, A. Yousef Mohamed, Ch. Yoo, E.-S. Park, S. Kim, S. Yoo, H.-K. Lee, D.-Y. Cho, C. Seong Hwang
ACS Appl. Mater. Interfaces 9, 47 (2017) 41387–41396
https://doi.org/10.1021/acsami.7b12946

[21] Local structure of epitaxial GeTe and $Ge_2Sb_2Te_5$ films grown on InAs and Si substrates with (100) and (111) orientations: An x-ray absorption near-edge structure study
A. V. Kolobov, P. Fons, M. Krbal, J. Tominaga, A. Giussani, K. Perumal, H. Riechert, R. Calarco, T. Uruga
J. Applied Physics 117 (2015) 125308
https://doi.org/10.1063/1.4916529

[22] *In situ* study of the crystallization in $GeTe_{0.26}Se_{0.74}$ thick film by synchrotron X-ray diffraction.
P. Armand, R. Escalier, J. Lizion, C. Mocuta, G. Silly, A. Piarristeguy
J. Alloys Compounds 953 (2023) 170034.
https://doi.org/10.1016/j.jallcom.2023.170034

[23] Phase-change materials for non-volatile memory devices: from technological challenges to materials science issues
P. Noé, C. Vallée, F. Hippert, F. Fillot, J.-Y. Raty
Semicond. Sci. Technol. 33 (2018) 013002.
https://doi.org/10.1088/1361-6641/aa7c25

[24] XPAD3: A new photon counting chip for X-ray CT-scanner
P. Pangaud, S. Basolo, N. Boudet, J.-F. Berar, B. Chantepie, P. Delpierre, B. Dinkespiler, S. Hustache, M. Menouni, C. Morel
Nucl. Instrum. Methods Phys. Res. A 571 (2007) 321–324.
https://doi.org/10.1016/j.nima.2006.10.092

[25] Detective quantum efficiency, modulation transfer function and energy resolution comparison between CdTe and silicon sensors bump-bonded to XPAD3S
K. Medjoubi, T. Bucaille, S. Hustache, J.-F. Bérar, N. Boudet, J.-C. Clemens, P. Delpierre and B. Dinkespiler
J. Synchrotron Rad. 17 (2010) 486–495.
https://doi.org/10.1107/S0909049510013257

[26] High-Energy Resolution Fluorescence Detected X-Ray Absorption Spectroscopy: A Powerful New Structural Tool in Environmental Biogeochemistry Sciences
O. Proux, E. Lahera, W. Del Net, I. Kieffer, M. Rovezzi, D. Testemale, M. Irar, S. Thomas, A. Aguilar-Tapia, E. F. Bazarkina, A. Prat, M. Tella, M. Auffan, J. Rose, J.-L. Hazeman
J. Environmental Quality, Special Section: Synchrotron Radiation-Based Method for Environmental Biogeochemistry 46 (2017) 1146-1157.
https://doi.org/10.2134/jeq2017.01.0023

[27] Investigation of the oxidation process in GeTe-based phase change alloy using Ge K-edge XANES spectroscopy
M. Krbal, A. V. Kolobov, P. Fons, K. Nitta, T. Uruga, J. Tominaga
Pure Appl. Chem. 91(11) (2019) 1769–1775
https://doi.org/10.1515/pac-2018-1229

[28] Ge K-Edge Extended X-Ray Absorption Fine Structure Study of the Local Structure of Amorphous GeTe and the Crystallization
Y. Maeda, M. Wakagi
Jpn. J. Appl. Phys. 30 (1991) 101-106
https://doi.org/10.1143/JJAP.30.101

[29] Phase Transitions in Germanium Telluride Nanoparticle Phase-Change Materials Studied by Time-Resolved X-Ray Diffraction
A.-K. U. Michel, F. Donat, A. Siegfried, O. Yarema, H. Fang, M. Yarema, V. Wood, Ch. R. Müller, D. J. Norris
J. Appl. Phys. 129 (2021) 095102

https://doi.org/10.1063/5.0032624

[30] In situ monitoring of stress change in GeTe thin films during thermal annealing and crystallization
B. Ben Yahia, M.S. Amara, M. Gallard, N. Burle, S. Escoubas, C. Guichet, M. Putero, C. Mocuta, M.-I. Richard, R. Chahine, C. Sabbione, M. Bernard, L. Fellouh, P. Noé, O. Thomas
Micro and Nano Engineering 1 (2018) 63–67
https://doi.org/10.1016/j.mne.2018.10.001

[31] X-ray absorption spectroscopy: EXAFS and XANES - A versatile tool to study the atomic and electronic structure of materials
E. E. Alp, S. M. Mini, M. Ramanathan
(ANL/APS/TM--7). United States (1990).

[32] Alteration of structural, electronic, and vibrational properties of amorphous GeTe by selenium substitution: An experimentally constrained density functional study
M. Micoulaut, A. Piarristeguy, O. Masson, R. Escalier, H. Flores-Ruiz, A. Pradel
Phys. Rev. B 104 (2021) 144204
https://doi.org/10.1103/PhysRevB.104.144204

[33] Selective detection of tetrahedral units in amorphous GeTe-based phase change alloys using Ge L3-edge x-ray absorption near-edge structure spectroscopy
M. Krbal, A. V. Kolobov, P. Fons, K. V. Mitrofanov, Y. Tamenori, J. Hegedüs, S. R. Elliott, J. Tominaga
Appl. Phys. Lett. 102 (2013) 111904
https://doi.org/10.1063/1.4794870

[34] Local order in binary Ge-Te glasses – an experimental study
P. Jóvári, A. Piarristeguy, A. Pradel, I. Pethes, I. Kaban, S. Michalik, J. Darpentigny, R. Chernikov
J. Alloys Compounds 771 (2019) 268-273
https://doi.org/10.1016/j.jallcom.2018.08.323

[35] Theoretical X-Ray Absorption Debye-Waller Factors
F. D. Vila, J. J. Rehr, H. H. Rossner, H. J. Krappe
Phys. Rev. B 76 (2007) 014301
https://doi.org/10.1103/PhysRevB.76.014301

[36] Comparative study of atomic arrangements in equiatomic GeSe and GeTe films before and after crystallization.
Y. G. Choi, S. Y. Shin, R. Golovchak, B.-K. Cheong, H. Jain,
J. Alloys Compounds 686 (2016) 273-280.
https://doi.org/10.1016/j.jallcom.2016.06.021